JOC The Journal of Organic Chemistry

Article

pubs.acs.org/joc

Photoconversion of β-Lapachone to α-Lapachone via a Protonation-Assisted Singlet Excited State Pathway in Aqueous Solution: A Time-Resolved Spectroscopic Study

Lili Du,[†,§] Ming-De Li,[†,§] Yanfeng Zhang,[†] Jiadan Xue,[‡] Xiting Zhang,[†] Ruixue Zhu,[†] Shun Cheung Cheng,[†] Xuechen Li,[†] and David Lee Phillips*[,†]

[†]Department of Chemistry, The University of Hong Kong, Hong Kong S.A.R., China

[‡]Department of Chemistry, Zhejiang Sci-Tech University, Hangzhou 310018, China

Supporting Information

ABSTRACT: The photophysical and photochemical reactions of β-lapachone were studied using femtosecond transient absorption, nanosecond transient absorption, and nanosecond time-resolved resonance Raman spectroscopy techniques and density functional theory calculations. In acetonitrile, β-lapachone underwent an efficient intersystem crossing to form the triplet state of β-lapachone. However, in water-rich solutions, the singlet state of β-lapachone was predominantly quenched by the photoinduced protonation of the carbonyl group at the β position (O_9). After protonation, a series of fast reaction steps occurred to eventually generate the triplet state α-lapachone intermediate. This triplet state of α-lapachone then underwent intersystem crossing to produce the ground singlet state of α-lapachone as the final product. 1,2-Naphthoquinone is examined in acetonitrile and water solutions in order to elucidate the important roles that water and the pyran ring play during the photoconversion from β-lapachone to α-lapachone. β-Lapachone can also be converted to α-lapachone in the ground state when a strong acid is added to an aqueous solution. Our investigation indicates that β-lapachone can be converted to α-lapachone by photoconversion in aqueous solutions by a protonation-assisted singlet excited state reaction or by an acid-assisted ground state reaction.

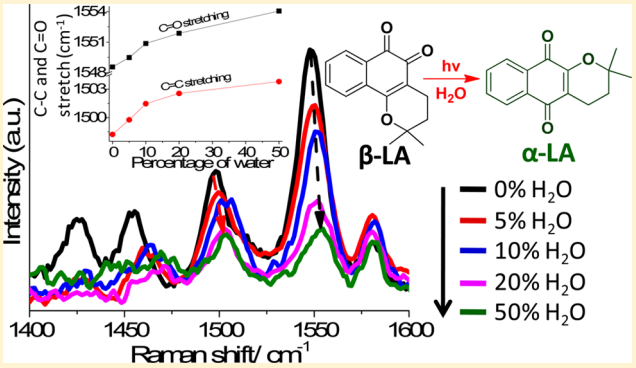

INTRODUCTION

β-Lapachone (β-LA) is an *ortho*-naphthoquinone obtained from the heartwood of *Tabebuia avellanedae*, which is mainly found in Brazil.[1,2] β-LA has been extensively studied due to its anticancer properties.[3−14] β-LA has been found to inhibit the growth of sarcoma tumors in mice[3] and to be cytotoxic to leukemia cells[4] and human cancers such as breast, colon, prostate, and lung.[5−14] The mechanism of the observed cytotoxicity in cancer cells appears to be due to NAD(P)H quinine oxidoreductase-1 performing a two-electron reduction of β-LA to produce its hydroquinone,[12,15−17] which may then generate reactive oxygen species to induce DNA damage that can lead to cell death.[18] Therefore, there has been some research effort conducted on the photoreactions of β-LA.[19−22]

Netto-Ferreira and co-workers[19,20] observed that β-LA is able to react with hydrogen donors, such as 2-propanol, 1,4-cyclohexadiene, 4-methoxyphenol, or indole, to form a corresponding ketyl radical. The low values observed for the hydrogen abstraction rate constant for β-LA when using 2-propanol and 1,4-cyclohexadiene as quenchers are independent of the solvent polarity, and this is thought to be due to the π,π* character of its excited triplet.[20] In the presence of alcohols, a semireduced radical (QH•), which is toxic to a normal cell,[18] was obtained under visible-light-induced photoreduction.[21,22] The probable mechanism for this photo-oxidation of the alcohols involves a H atom abstraction quenching of the excited state followed by an electron transfer/proton transfer sequence in which ground state β-LA is reduced. Lower limiting efficiencies for the photoreduction of β-LA by the alcohols are attributed to inefficiencies of the net H atom transfer in the quenching step.[21] In addition, both triplet states of β-LA and β-LA-3-sulfonic acid were efficiently quenched by amino acids and nucleobases or nucleosides induced by an initial electron transfer and followed by a fast proton transfer.[19,23] The quinone cation radicals were also detected in the study of β-lapachone derivatives.[24,25]

Although a number of studies have examined β-LA in organic solvents, the phototoxicity mechanism of β-LA toward cancers cells remains poorly understood because the organic solution conditions are very different from those of the biological environment. Therefore, it will be useful to investigate the photophysics and photochemistry of β-LA in aqueous solutions that are more relevant to the actual solvent environment in

Received: January 13, 2015
Published: July 2, 2015

DOI: 10.1021/acs.joc.5b00086
J. Org. Chem. 2015, 80, 7340−7350

biological systems. To the best of our knowledge, we report here the first time-resolved spectroscopic study of the photoinduced reaction(s) of β-LA in aqueous solutions. Proton transfer reactions and protonation are fundamental classes of reactions in chemical transformations and play an important role as fundamental processes throughout nature.[26] Photoinduced intermolecular proton transfer reactions are also ubiquitous in numerous chemical and biological processes. Results from some previous studies of selected aromatic carbonyl compounds in aqueous solutions found that photoinduced protonation of a ketone may often open some novel photochemical reactions dependent on the water concentration and acidity of the solutions.[27−29] Since β-LA contains a couple of ketone groups, it may exhibit similar behavior in aqueous solutions.

We are pleased to report in this paper femtosecond and nanosecond transient absorption (fs-TA and ns-TA) and nanosecond time-resolved resonance Raman (ns-TR^3) spectroscopic methods to investigate the early events taking place for β-LA after photoexcitation in aqueous solutions. As far as we know, this is the first time that fs-TA, ns-TA, and ns-TR^3 experiments have been performed on β-LA in different acetonitrile (MeCN)/H_2O mixture solutions in order to investigate the role of water on the excited states, intermediates, and dynamics of reactive intermediates that are involved in the photochemistry of β-LA. To help determine the geometries and vibrational spectra of the intermediate species and assignments of the experimental vibrational bands, density functional theory (DFT) calculations were done using the B3LYP methods with a 6-311G** basis set for all of the species examined here. The structure and properties of the triplet state of β-LA (β-^{3}LA) are also briefly discussed. In order to distinguish the important role of the pyran ring in the photochemistry, the photoreaction of the parent compound 1,2-naphthoquinone (NQ) that does not contain a pyran ring (see Scheme 1) was also studied by time-resolved spectroscopy methods in both MeCN and aqueous solutions and compared to the results found for β-LA here. Our time-resolved spectroscopy results indicate that a photoinduced protonation of the carbonyl group at the β position takes place for the singlet excited state of β-LA with the assistance of water in aqueous solutions. This protonation initiates a series of processes that lead to the conversion of some β-LA to α-LA in water-rich solutions and acidic aqueous solutions. This photoinduced protonation reaction provides insight into the role of water in the cytotoxicity and phototoxicity of β-LA in biological systems and its potential use in photodynamic therapy applications.

Scheme 1. Structures of β-LA and NQ

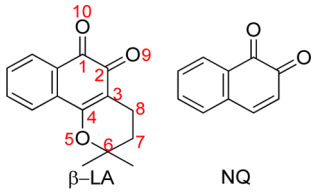

RESULTS AND DISCUSSION

Transient Absorption and Ns-TR^3 Spectroscopic Study of NQ and β-LA in MeCN. Fs-TA spectra were obtained for the parent compound NQ in MeCN and are shown in Figure 1. The spectra at early (Figure 1a) and later delay times (Figure 1b) are given separately to more easily discern the spectral changes that take place on different time scales. After irradiation by 267 nm light, the ground state of NQ is transferred to a higher excited singlet state S_n, and the very early time TA spectra are assigned to the relaxation from the S_n to S_1 state.[30] The initial species that appears at 370 (sharp band) and 480 nm (broad band) at 2 ps can be assigned to S_1 to S_n absorption from the singlet excited state of NQ. The time constant for internal conversion from S_n to S_1 is within the instrument response time and will not be discussed here. In Figure 1b, the bands at 370 and 480 nm are noticeably shifted with time toward a longer wavelength, ultimately yielding a sharp band at 375 nm and a broad absorption band centered at 593 nm that extends from below 460 nm to above 680 nm. An isosbestic point at 535 nm indicates a dynamical conversion between two distinct states, and the spectrum recorded after 30 ps appears identical to that assigned previously to the triplet state of NQ (^{3}NQ).[19,31] From the inserted graph in Figure 1b, the kinetics of the 480 nm decay can be fitted simultaneously by a single-exponential function with a 7 ps time constant, which is very close to the ISC time constant of benzophenone recorded in MeCN.[32,33] This indicates that the spectral transformation observed here is due to the ISC conversion from the lowest singlet (S_1) the triplet (T_1) of NQ.

From Figure 2, it can be seen that the temporal evolution of the early time spectra for β-LA obtained after 267 nm excitation in MeCN is very similar to that of NQ. To clearly discern the spectral changes on different time scales, the spectra of the early

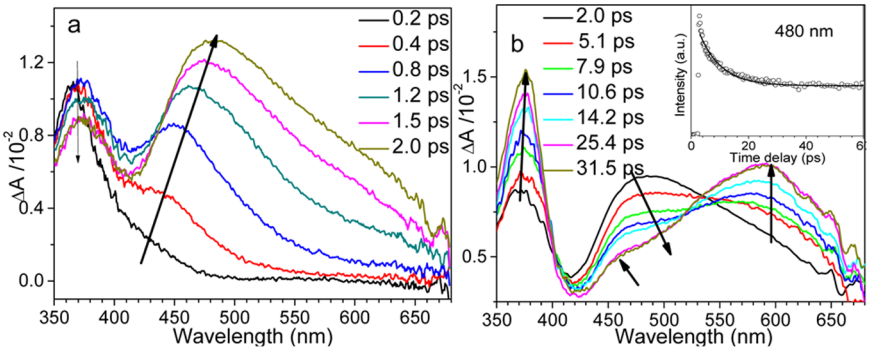

Figure 1. Fs-TA spectra of NQ in MeCN solution obtained after 266 nm excitation from 0.2 to 2.0 ps (a) and 2.0 to 31.5 ps (b). Temporal dependence of the transient absorption spectra for NQ recorded at early picosecond times at 480 nm is inserted at the top of the right panel. The solid lines indicate the best-fit kinetics to the experimental data points.

DOI: 10.1021/acs.joc.5b00086
J. Org. Chem. 2015, 80, 7340−7350

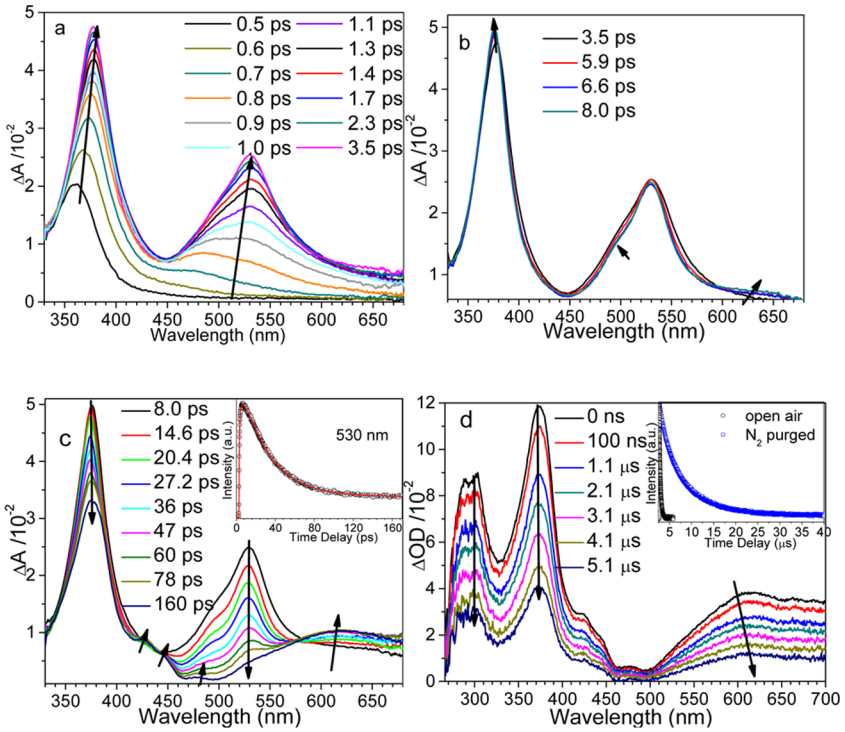

Figure 2. (a–d) Fs-TA and ns-TA spectra of β-LA in neat MeCN solvent acquired after 267 nm irradiation. Kinetics of the characteristic fs-TA absorption bands observed at 530 nm are inserted at the top of (c). Kinetics of the characteristic ns-TA absorption bands observed with nitrogen saturated (left) and air saturated (right) at 373 nm and excited by 267 nm in MeCN solvent are inserted at the top of (d). The solid lines indicate the kinetics fitting to the experimental data points.

(before 3.5 ps), 3.5–8 ps, and later (8–160 ps) times are given separately in Figure 2. It can be seen that both the 370 and 530 nm bands grow in rapidly within 3.5 ps (see Figure 2a). Later (Figure 2b), the 374 nm band increases in intensity slightly, while the 530 nm band does not change much and the shoulder at 494 nm appears. Meanwhile, both of the two bands blue shift slightly and become narrower. In the next 160 ps (Figure 2c), with the decrease in intensity of the 530 and 370 nm bands, another broad absorption band (around 610 nm) appears within 100 ps and an isosbestic point at ~570 nm is seen, which indicates a dynamical conversion between two distinct states. The two transient absorption bands at 373 and 610 nm as well as the three small bands around 400–500 nm appear to be stable until 3 ns. Based on the fs-TA results of NQ and the transient absorption features of the triplet of NQ in MeCN, the transient absorption bands after 160 ps are likely to be due to the β-^{3}LA intermediate. From the inserted graph shown in Figure 2c, the kinetics of the 530 nm decay can be simulated satisfactorily by a triexponential function with the time constants of 524 fs (τ_1), 5 ps (τ_2), and 29 ps (τ_3), weighted by different proportionality factors. The spectrum at very early time (from 0.5 to 3.5 ps in Figure 2a) is assigned to an internal conversion from the S_n to S_1 (n,π^*), whose lifetime is 524 fs. Then, the S_1 state is thermalized by vibrational cooling in 5 ps, as evidenced by the narrowing and blue shifting of the bands. With the reduction of the S_1 signal, the subsequent changes in the spectra are mainly attributed to the S_1 (n,π^*) to T_1 (π,π^*) ISC process (τ_3 = 29 ps) that leads to the increase of the transient absorption at 610 nm, which corresponds to the T_1 to T_n transition with maxima at 373 and 610 nm in neat MeCN solvent. Spectra at later delay times resemble those obtained from nanosecond laser flash photolysis spectra of β-LA in MeCN and the time evolution analysis of the absorbance at 373 nm of β-LA in MeCN under open air and nitrogen-purged conditions (these results are given in Figure 2d). The observed quenching by oxygen provides further evidence that the species observed in the later fs-TA and ns-TA is a triplet species in nature. The $^3\beta$-LA intermediate was reported to have a sharp band 380 nm and a broad absorption band at 650 nm in MeCN,[19,20] which is analogous to the observation in our fs-TA and ns-TA experiments.

Time-dependent DFT (TD-DFT) calculations were carried out on the singlet and triplet states of NQ and β-LA in order to predict their UV–vis spectra, and these results are shown in Table 1S of the Supporting Information. The frontier orbitals of NQ and β-LA obtained from these calculations are shown in Figure 1S of the Supporting Information. As seen in Table 1S, the experimental data are consistent with the calculation-predicted spectra of the excited states. The first singlet states of both molecules are calculated to have two strong absorption bands in the visible region, which are also observed in the experimental results: (1) 349, 331 nm transitions corresponding to a transition from the benzyl ring to the dione ring (LUMO) for both NQ and β-LA, which explains the almost identical wavelength (370 nm) for these two compounds in the experimental spectra; and (2) 441, 471 nm transitions due to π,π^* transitions for NQ and β-LA with little difference, while the pyran ring of β-LA contributes to the transition on the higher wavelength where the band is 50 nm red-shifted for β-LA (530 nm) compared to the analogous band for NQ (480 nm) in the experimental spectra.

In an attempt to characterize the vibrational structure and properties of the intermediates involved for β-LA in MeCN after photoexcitation, ns-TR^3 experiments were done using 266 nm as the pump laser wavelength and 368.9 nm as the probe laser wavelength for β-LA in MeCN. Figure 2S displays the ns-

DOI: 10.1021/acs.joc.5b00086
J. Org. Chem. 2015, 80, 7340–7350

TR^3 spectra of β-LA in MeCN, and mainly one species was observed. Fs-TA and ns-TA experiments suggest that the intermediate detected in the nanosecond time range is the β-^{3}LA intermediate. DFT calculations were done to predict the Raman spectrum of β-^{3}LA, and the calculated result was compared with the experimental TR^3 spectrum obtained at 10 ns in Figure 3. Examination of Figure 3 reveals that the

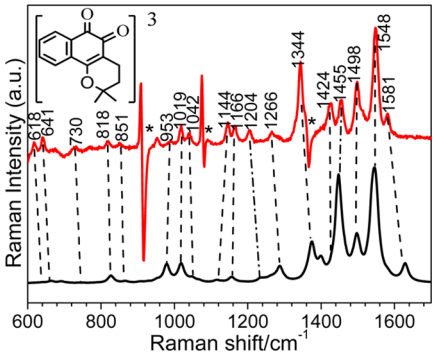

Figure 3. Comparison the experimental resonance Raman spectrum (10 ns time delay) of β-LA obtained in pure MeCN (pump 266 nm, probe 368.9 nm) with the DFT-calculated normal Raman spectrum of β-^{3}LA. The star symbols indicate the regions affected by solvent subtraction artifacts.

calculated Raman spectrum shows reasonable agreement with the experimental TR^3 spectrum for the β-^{3}LA species in terms of the vibrational frequency pattern of the two spectra. The slight differences between the relative intensity patterns of the experimental spectrum and the calculated spectrum can be attributed to the experimental spectrum being resonantly enhanced while the calculated spectrum is a normal Raman spectrum. Most of the Raman bands seen in the TR^3 spectra of β-^{3}LA are due to the vibrations associated with the ring C−C stretch and C−H bend motions. Six major Raman bands at 1581, 1548, 1498, 1455, 1424, and 1344 cm^{-1} were observed. The 1581, 1548, and 1344 cm^{-1} Raman bands are mainly due to the ring C−C stretch, C═O stretch, and H−C−H scissor vibrational modes. The 1498 cm^{-1} Raman band is associated with a C═O stretch and a C−H in-plane rocking of the ring vibrational modes. The 1440 cm^{-1} Raman band is due to a combination of the C−O stretching and C−H wagging modes. The 1424 cm^{-1} Raman feature is attributed by the C−H scissoring mode.

For aromatic carbonyl compounds, the electronic configuration of the T_1 state determines the T_1 state's reactivity toward the hydrogen abstraction reaction with hydrogen donor reagents. Two types of T_1 states, dominated respectively by n,π^* and π,π^* character, have been identified to be responsible for the differences in the T_1 photophysical and photochemical behavior.[34−36,38] A T_1 state with mainly n,π^* nature exhibits a high efficiency for a hydrogen abstraction reaction, whereas a triplet state with a π,π^* nature is barely reactive for that type of reaction. Previous TR^3 and TRIR studies found that the frequency of the C═O stretch mode appears in the 1400−1600 cm^{-1} range for a π,π^* predominant character triplet state, while it is in the 1200−1400 cm^{-1} region for a typical n,π^* nature triplet state.[37−40] As illustrated above, the C═O stretch frequencies for the β-^{3}LA state are at 1581 and 1498 cm^{-1}, and this indicates that the β-^{3}LA intermediate possesses mainly a π,π^* electronic configuration. This may account for the low efficiency of the hydrogen abstraction for β-LA when using 2-propanol and 1,4-cyclohexadiene as quenchers.[20,21]

Transient Absorption Study of β-LA and NQ in MeCN and H_2O Mixed Solutions. *Protonation Accounts for the Decay of the Singlet Excited State of β-LA.* Fs-TA spectra of NQ excited by 267 nm in 1:1 MeCN/H_2O mixed solution were obtained and are shown in Figure 3S (Supporting Information). It is obvious that the temporal evolution of the early time spectra is almost the same as that in neat MeCN, with bands at 370 and 480 nm appearing as the singlet of NQ (^{1}NQ) that then undergoes the ISC process (7 ps) to generate its triplet excited state (^{3}NQ) with absorption bands at 375 and 593 nm. Figures 4S and 5S (Supporting Information) and Figure 4a display the fs-TA results for β-LA in 9:1 MeCN/H_2O, 4:1 MeCN/H_2O, and 1:1 MeCN/H_2O mixed solutions excited at 267 nm. Similar to the fs-TA results obtained in neat MeCN solution, bands at 370 and 530 nm grow in rapidly within 3 ps in the MeCN/H_2O mixed solutions (see Figure 4S in the Supporting Information), which are due to an internal conversion process from S_n to S_1 of β-LA. In Figure 5Sa (Supporting Information), with decreasing intensity of the bands at 370 and 530 nm, the band at 610 increases slightly without an obvious isosbestic point in 9:1 MeCN/H_2O mixed solvent. However, no obvious increase in intensity at 610 nm was detected in the 4:1 MeCN/H_2O mixed solvent in Figure 5Sb (Supporting Information). This clearly indicates that the generation of β-^{3}LA was inhibited with the presence of H_2O. The transient absorption at 610 nm almost does not decay any more from 3.7 to 126.7 ps (see Figure 5Sa, Supporting Information); this demonstrates that some β-^{1}LA still undergoes the ISC to transform into the β-^{3}LA while a small portion of β-^{1}LA undergoes an unknown reaction with water molecules.

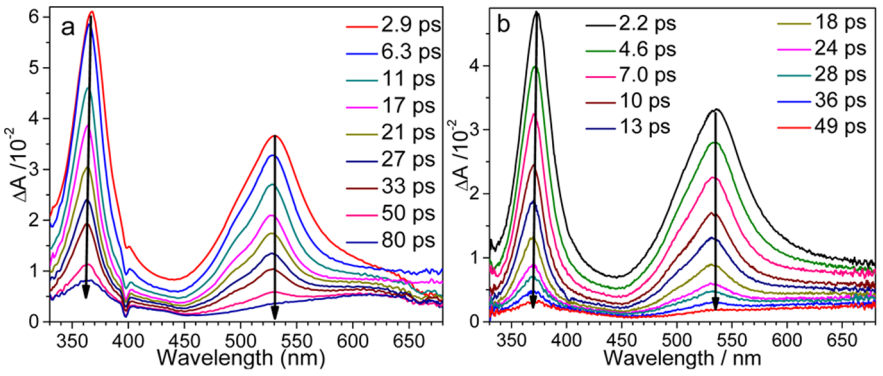

Figure 4. Fs-TA spectra of β-LA in (a) 1:1 MeCN/H_2O and (b) 1:1 MeCN/H_2O (pH 0) mixed solutions obtained after 267 nm excitation.

DOI: 10.1021/acs.joc.5b00086
J. Org. Chem. 2015, 80, 7340−7350

When the concentration of water increases to 50% (1:1 MeCN/H_2O mixed solvent), no increase in intensity at 610 nm can be observed with the significant decrease of intensity of both bands at 370 and 530 nm (see Figure 4a). To confirm the participation of water molecules, Figure 5 presents the singlet

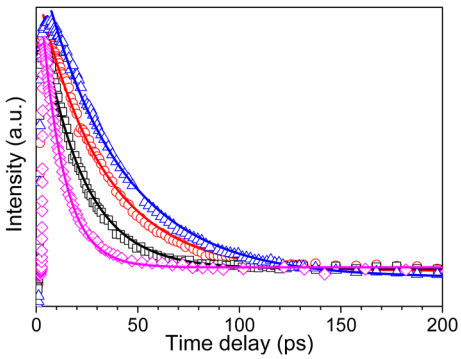

Figure 5. Temporal dependences of the transient absorption intensity for β-LA in 9:1 MeCN/H_2O (Δ), 4:1 MeCN/H_2O (○), 1:1 MeCN/H_2O (□), and 1:1 MeCN/H_2O (pH 0) (◊) mixed solutions at 530 nm are shown. Solid lines indicate fitting using a single-exponential function to fit the experimental data.

decay dynamics at 530 nm of β-LA in the four solvents of varying water concentration. The time constants for the singlet decay dynamics are 38, 32, and 20 ps in 9:1 MeCN/H_2O, 4:1 MeCN/H_2O, and 1:1 MeCN/H_2O mixed solutions, respectively. These results show that the rate of the unknown reaction of β-LA with water in the different aqueous solutions increases noticeably with the increasing concentration of water because the β-^{1}LA decays much faster than that obtained in the lower water concentration solutions. This indicates that the β-^{1}LA intermediate may be involved in a reaction with H_2O. The high reactivity of the *ortho*-diketones gives rise to the high potential in the low excited state reduction potential.[41] Solvent polarization also induces a small barrier to proton transfer for the zero-point motion.[42] Therefore, protonation can likely occur from β-^{1}LA in aqueous solution, as since Hooker[43] has already pointed out that conversion from β-LA into α-LA can take place in the presence of hydrogen chloride on the ground state potential surface. It appears that the protonation of the carbonyl group (O_9) may also be the driving force to promote the transformation from β-LA into α-LA on an excited state potential surface. Since the ISC process of NQ is not affected by the increase of the concentration of water molecules, this implies that the pyran ring of β-LA determines the reaction between β-^{1}LA and water molecules. Given that the protonation of the carbonyl group may drive β-LA into α-LA in the acidic aqueous solution on the ground state,[43] the excited state of β-LA can also probably be easily protonated compared to the ground state of β-LA. Fs-TA results indicate that the lifetime of β-^{1}LA will gradually decrease with the increase of the concentration of water. This reveals that β-^{1}LA may be protonated even in the neutral high water concentration solutions, and this is consistent with observations that benzophenone is a very weak base in the ground state and its protonation requires a very strong acid; however, the acidity of the conjugate acid, $pK_a(S_0)$ = 4.7, is reduced by 4 orders of magnitude in the excited triplet state, $pK_a(S_1)$ = 0.4.[27,44] This would suggest that the protonation of the excited state of β-LA would be much easier than for its ground state. Figure 6S (see Supporting Information), Figure 4b, and Figure 5 (◊) display the fs-TA spectra and kinetics for β-LA in 1:1 MeCN/H_2O (pH = 0) mixed solutions excited at 267 nm. Examination of Figure 4b indicates that the bands at 370 and 530 nm in pH 0 acidic solution decrease in intensity much faster than those in the 50% water solution. As shown in Figure 5, the time constant for the singlet decay dynamics in the pH 0 solution is about 11 ps, which is much shorter than that obtained in the 50% water neutral mixed solutions. This provides a direct piece of evidence to support that the β-^{1}LA may be protonated in aqueous solutions.

Competition between Intersystem Crossing into β-^{3}LA in Lower Water Concentration Solutions and Protonation Conversion into α-^{3}LA in Water-Rich Solutions. Ns-TA experiments were also performed for β-LA in different aqueous solutions. The ns-TA spectra and temporal evolution at 373 nm in the (a) MeCN, (b) 95:5 MeCN/H_2O, (c) 9:1 MeCN/H_2O, (d) 8:2 MeCN/H_2O, (e) 7:3 MeCN/H_2O, and (f) 1:1 MeCN/H_2O mixed solutions are presented in Figures 7S−9S in the Supporting Information. The time constants for the transient species' decay dynamics obtained from the ns-TA spectra are summarized in Table 1 for β-LA in the MeCN and mixed

Table 1. Time Constants of the Decay Dynamics at 373 nm in Different Solutions

solvent	MeCN	MeCN/H_2O	MeCN/H_2O	MeCN/H_2O	MeCN/H_2O	MeCN/H_2O
t/τ		95:5	9:1	8:2	7:3	1:1
N_2 purged						
τ_1	6.8 μs	2.6 μs	2.1 μs	2.0 μs	3.3 μs	2.7 μs
τ_2		5.8 μs	4.5 μs	3.8 μs		
open air						
τ	264 ns	327 ns	378 ns	427 ns	463 ns	695 ns

aqueous solvents with varying water content. The time constants obtained in the open air condition are dramatically shorter than that obtained in a nitrogen-purged condition. This indicates that the transient species observed in the ns-TA experiments have triplet character. The different lifetimes in different solvents under open air are caused by the different concentration of oxygen dissolved in the solutions; the lifetime is 264 ns in the neat MeCN, while the lifetime is 695 ns in 50% water concentration solution; this is because the oxygen has a higher dissolve ability in MeCN than in water solution. It is interesting to note that, for solvents with water content larger than 30% and in the neat MeCN solvents, only one time constant can be obtained (see Table 1), which is in accordance with the results achieved in the fs-TA spectra recorded in 1:1 MeCN/H_2O mixed solution, where the β-^{1}LA is quenched by the protonation and no β-^{3}LA is generated, while in neat MeCN solvent, the β-^{1}LA completely transforms into the β-^{3}LA by ISC. Therefore, the 6.8 μs is the lifetime of β-^{3}LA, while the 3.3 and 2.7 μs accounts for the lifetime of a new species that has a triplet character (generated by the protonation of β-^{1}LA). In less than 30% water solution, there are two time constants that can be obtained by a biexponential fitting of the dynamics of 373 nm. According to the preceding interpretation, the short time constants (2.6, 2.1, and 2.0 μs obtained in 5, 10, and 20% water solution, respectively) are associated with the new species produced by the protonation of the singlet excited state of β-LA; in contrast, the longer time constants (5.8, 4.5, and 3.8 μs) are the lifetime of the β-^{3}LA species.

DOI: 10.1021/acs.joc.5b00086
J. Org. Chem. 2015, 80, 7340−7350

According to the discussion above, the transient species with the longer lifetime is β-^{3}LA, whose formation decreases as the concentration of water increases. The dependence of the transient species' decay dynamics on water concentration reflects the effect of the local solvent environment on the triplet quenching process. The different lifetimes between the nitrogen-purged and open air conditions indicate that the species obtained in the ns-TA in 1:1 MeCN/H_2O mixed solution may be triplet in nature. Figure 6 shows the ns-TA

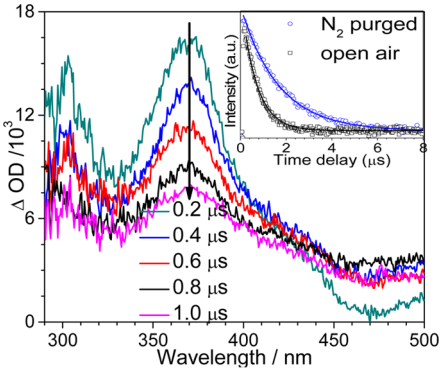

Figure 6. Ns-TA spectra of β-LA in 1:1 MeCN/H_2O mixed solution obtained after 266 nm excitation. Inset: Transient absorption decay of β-LA in 1:1 MeCN/H_2O mixed solution purged with N_2 (○) and saturated air (□). The solid lines indicate the kinetics fitting to the experimental data points.

spectra acquired after photolysis of β-LA in 1:1 MeCN/H_2O mixed solution under open air. Only one species is obtained through the ns-TA experiment, which displays absorption maxima at 304, 374, and 440 nm. The transient spectra here are almost the same as the transient absorption of the triplet state of α-LA (α-^{3}LA) obtained in MeCN by Netto-Ferreira[45] with a small shift in the wavelength. Therefore, the character of the transient species observed in 50% water solution can probably be assigned to the α-^{3}LA intermediate.

Confirmation of the Assignment of α-^{3}LA by ns-TR^3 Spectra. To gain structural information for the reactive intermediates, ns-TR^3 experiments were performed for β-LA in different aqueous solutions. Figure 7 displays the ns-TR^3 spectra at 10 ns of β-LA in (a) MeCN, (b) 95:5 MeCN/H_2O,

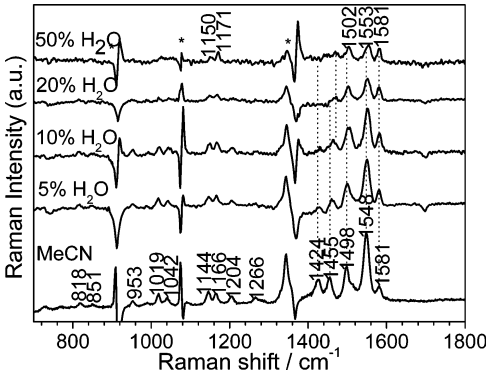

Figure 7. Ns-TR^3 spectra of β-LA obtained with 266 nm excitation and a 368.9 nm probe wavelength in (a) MeCN, (b) 95:5 MeCN/H_2O, (c) 9:1 MeCN/H_2O, (d) 8:2 MeCN/H_2O, and (e) 1:1 MeCN/H_2O mixed solutions at 10 ns time delay. The sharp features labeled by (*) are due to solvent subtraction artifacts and/or stay light.

(c) 9:1 MeCN/H_2O, (d) 8:2 MeCN/H_2O, and (e) 1:1 MeCN/H_2O mixed solutions using a 368.9 nm probe wavelength and a 266 nm pump wavelength. In the MeCN solvent, the main resonance Raman bands of β-LA are at 641, 818, 953, 1019, 1042, 1144, 1166, 1204, 1266, 1344, 1424, 1455, 1498, 1548, and 1581 cm^{-1}. Based on the study of β-LA in MeCN, the transient species detected at 10 ns could be assigned to β-^{3}LA. In the 50% water solution, the main resonance Raman bands appear at 1150, 1171, 1469, 1502, 1553, and 1581 cm^{-1}. According to the ns-TA study of β-LA, the transient species detected in the 50% aqueous solution are likely to be the α-^{3}LA species. Thus, DFT calculations were conducted to predict the normal Raman spectra of α-^{3}LA, and Figure 8 displays the comparison between the experimental

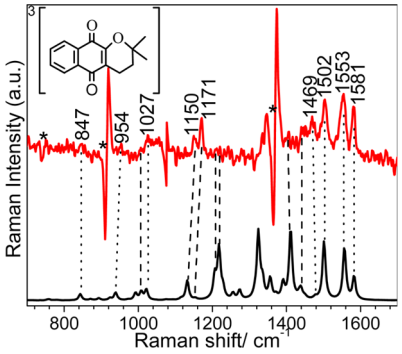

Figure 8. Comparison the experimental resonance Raman spectra (10 ns time delay) of β-LA obtained in 1:1 MeCN/H_2O (pump 266 nm, probe 368.9 nm) with the DFT-calculated normal Raman spectrum of α-^{3}LA.

TR^3 spectrum obtained at 10 ns and the B3LYP/6-311G** DFT-calculated normal Raman spectrum of α-^{3}LA. Inspection of Figure 8 shows that there is excellent agreement between the vibrational frequency patterns of the calculated normal Raman spectrum and the ns-TR^3 spectrum. The dotted lines indicate the correspondence of the vibrational features in the calculated and experimental spectra in Figure 8. This further indicates that the transient species observed in the nanosecond time scale can be assigned to α-^{3}LA. To better understand the ns-TR^3 spectra variation in the different solutions, DFT calculations have been employed to optimize the structures and predict normal Raman spectra of β-^{3}LA and α-^{3}LA. The optimized structures of β-^{3}LA and α-^{3}LA are displayed in Figure 10S. The bond lengths of C_{11}–C_{12}, C_{14}–C_{15}, C_4–O_5, C_1–O_{10}, and C_2–O_9 are 1.417, 1.435, 1.329, 1.249, and 1.259 Å for β-^{3}LA and 1.407, 1.419, 1.254, 1.254, and 1.315 Å for α-^{3}LA, respectively. The DFT calculations indicate that the Raman bands of 1498 and 1548 cm^{-1} are mainly contributed from the C–C stretch of C_{11}–C_{12} and C_{14}–C_{15} and C═O stretch of C_1–O_{10} and C_2–O_9 for β-^{3}LA. The bond lengths of C_{11}–C_{12}, C_{14}–C_{15} (1.407 and 1.419 Å), and C_4–O_5 (1.254 Å) for α-^{3}LA are shorter than those of C_{11}–C_{12}, C_{14}–C_{15} (1.417 and 1.435 Å), and C_1–O_{10} (1.259 Å) for β-^{3}LA. This suggests that Raman bands contributed by the C–C stretch of C_{11}–C_{12} and C_{14}–C_{15} and C═O stretch of C_1–O_{10} and C_2–O_9 will shift up to higher wavenumber when β-^{3}LA converts into α-^{3}LA. This is consistent with the ns-TR^3 experimental Raman spectra changes. Figure 7 shows that the Raman bands at 1498 and 1548 cm^{-1} shifted to 1502 and 1553 cm^{-1}, and there is also a remarkable change in their relative intensity as there is an

DOI: 10.1021/acs.joc.5b00086
J. Org. Chem. 2015, 80, 7340–7350

Scheme 2. Proposed Protonation Photoinduced Conversion Mechanism from β-LA into α-LA in Aqueous Solutions

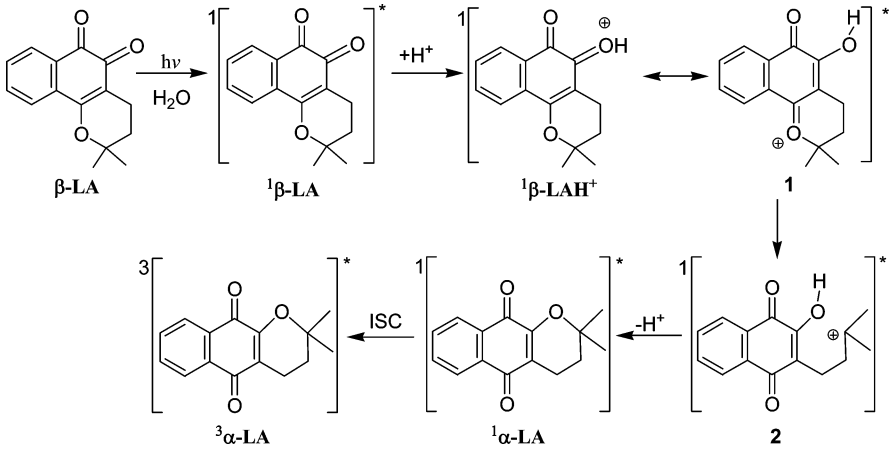

increase of the water concentration. Furthermore, the 1424 and 1455 cm^{-1} Raman bands were observed in MeCN solvent, while they almost disappear in the 50% water solution. The Raman bands at 1424 and 1455 cm^{-1} are associated with the C−O stretch of C_4-O_5 (1.329 Å) for β-^{3}LA. When the increase in the water concentration reaches 50%, some α-^{3}LA species are generated and the cleavage of the C_6-O_5 bond gives the C_4-O_5 double bond character. This causes the Raman bands associated with the single-bond C−O stretch of C_4-O_5 (1.329 Å) for β-^{3}LA to disappear. In summary, the ns-TR^3 spectra changes in the different solutions are in accordance with the features of the optimized structures and DFT-calculated normal Raman spectra for β-^{3}LA and α-^{3}LA. This demonstrates that the transient species detected in the 50% water solution are convincingly assigned to the α-^{3}LA species.

Discussion of the Photochemical Reaction Mechanism of β-LA in Aqueous Solutions. Based on the data presented above, the proposed photochemical reaction pathways of β-LA in aqueous solutions are shown in Scheme 2. After photoexcitation in MeCN, both the first singlet excited state of β-LA and NQ undergo an ISC process to transform into the β-^{3}LA and ^{3}NQ species with time constant of 7 and 29 ps, respectively. In the 50% water solution, the photochemical reaction pathway of NQ is the same as that observed in the MeCN solvent. However, β-LA exhibits a different photochemical reaction in the aqueous solutions compared with the one observed in MeCN solvent. In the 50% water solution, the carbonyl group at the β position of first excited state of β-LA tends to be quenched by protonation. The fs-TA results of β-LA in the pH 0 acidic solution further indicate that the protonation may accelerate the quenching of the β-^{1}LA species. Therefore, the excited state of β-LA is first protonated in the aqueous solution or acidic solution, and then the resonant species of the protonation of the excited state of β-LA will promptly transform into the excited state of α-LA by the cleavage of the O_5-C_6 bond and the cyclization reaction to form the singlet excited state of α-LA. The singlet excited state of α-LA is a very short-lived intermediate, which was quickly consumed through an intersystem crossing and formed the triplet state of α-LA. This apparently occurs very fast, and the singlet excited state of α-LA was not resolved under the resolution of the present fs-TA experiments. Finally, only the triplet state of α-LA was detected by ns-TA and ns-TR^3 experiments.

Given that Hooker[43] and Ettlinger[46] reported that the ground state of β-LA can be thermodynamically converted into α-LA in the presence of hydrogen chloride. To explore the formation of the ground singlet state of α-LA, DFT calculations were carried out on the cyclization reactions from the protonated β-LA to ground singlet state of α-LA. Figure 10S shows the optimized structures of the reactant complex (RC_n), transition state (TS_n), and product complex (PC_n) (for which n represents the sequence of the reaction steps) obtained from B3LYP/6-311G** calculations. Selected bond lengths are given in the optimized structures shown in Figure 11S. These DFT computations found that formation of the ground singlet state of α-LA needed a pathway through two steps. The first step involves the carbocation attacking the oxygen (O_9) of the alcohol group, and the second step involves a deprotonation to produce the singlet state of α-LA. The energy barriers of the two steps are 2.94 and 1.87 kcal/mol, respectively (see Figure 9). The very small energy barriers for these two steps

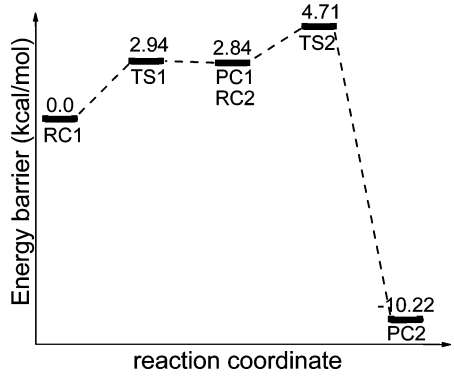

Figure 9. Reactive energy profiles obtained from (U)B3LYP/6-311G** calculations are shown from the carbocation 2 transient to the singlet state of α-LA (see text for more details).

demonstrate that the cyclization reactions easily proceed in acidic aqueous solutions. Using hydrogen chloride as an acidic catalyst for β-LA to prepare α-LA, Ettlinger reported 70% conversion efficiency, and the final product was only characterized by its melting point and an elemental analysis.[48] In order to confirm the conversion from β-LA into α-LA in the acidic solution, we repeated the experimental procedure and obtained a 90% conversion efficiency from β-LA to α-LA. The final product was characterized by NMR, mass spectra, and

DOI: 10.1021/acs.joc.5b00086
J. Org. Chem. 2015, 80, 7340−7350

Scheme 3. Alternatively Proposed Mechanism from β-LA into α-LA in Aqueous Solutions

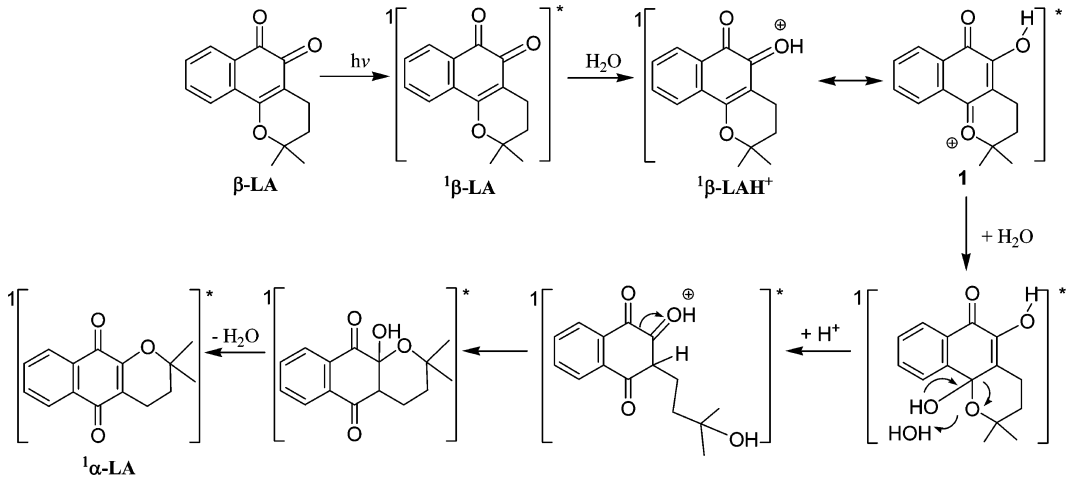

UV−vis absorption spectra, which are displayed in the Supporting Information, and the NMR and mass spectra of the final product agree well with the literature ones reported for the spectroscopic and spectrometric properties of α-LA.[45,47] Since protonation of the ground state of β-LA in the acidic solution efficiently undergoes the decyclization and cyclization to produce α-LA, it is believed that excited state of β-LA (β-^{1}LA) will also able to convert into α-LA in the high water concentration solutions or acidic aqueous solution. As mentioned above, the time-resolved spectra results demonstrated that the β-^{1}LA species undergo ISC to form the β-^{3}LA species in MeCN in low water concentration solutions, while the β-^{1}LA mostly convert into the α-^{3}LA in high water concentration solutions or acidic solution. This implies that water plays a very important role in the conversion process, and that the protonation of the β-^{1}LA species enables the transformation from β-^{1}LA into the α-^{3}LA intermediate observed in the ns-TA and ns-TR^3 spectra that eventually forms the α-LA final product. This implies that the water environment may significantly change the photochemical pathways of β-LA. Our previous studies on Ketoprofen (KP) also found that an increase in the water concentration may shuttle a proton from the carboxyl group to the carbonyl group via the water hydrogen bonded network that could lead to KP undergoing a photodecarboxylation reaction in neutral high water concentration solutions.[29,48,49] This makes KP in aqueous solutions exhibit a different photochemical pathway compared with that obtained in a neat MeCN or low water concentration solutions.

β-LA may also possibly be converted into α-LA by another alternative pathway. The protonation of singlet excited state β-LA ($^1\beta$-LAH$^+$) could be susceptible to conjugate β-addition of water at C_6, which then leads to formation of a hemiacetal (see Scheme 3). Ketonization of the C_6 carbon with the departure of the alcohol side chain produces a benzo-1,2,4-trione with a 2-methyyl-2-hydroxybutanyl side chain. The hydroxyl group then bonds at the C_2 carbonyl followed by dehydration to form α-LA. In order to assess the susceptibility of the conjugate β-addition of water at C_6, the reaction energy profile of β-addition of water at C_6 was scanned for the protonated β-LAH$^+$ species. The computational result indicates that the energy surface of the β-addition of water at C_6 for the protonated β-LAH$^+$ species is an endothermic reaction throughout the scan (see Figure 12S); hence, it can be concluded that the β-addition of water at C_6 is not very likely to occur in a thermodynamic sense. However, kinetically, we cannot exclude the possibility of the conjugate β-addition of water at C_6 because the protonated β-LAH$^+$ species might occur to some degree. However, the DFT calculation results reveal that the bond lengths of O_5-C_4 and O_5-C_6 are 1.346 and 1.472 Å, respectively, for the ground state of β-LA, while the bond lengths of O_5-C_4 and O_5-C_6 are 1.293 and 1.526 Å, respectively, after the protonation of ground state of β-LA (see Figure 13S). This reveals that the protonated ground state of β-LA tends to undergo the cleavage of the O5−C6 bond more easily. Winter and co-workers reported that some unstabilized carbocations have been found to have structurally nearby, low-energy conical intersections that are often favored for photochemical heterolysis, whereas some stabilized carbocations have been found to have high-energy, unfavorable conical intersections, which may be favored for thermal heterolysis.[50] For the formation of the carbocation intermediates in Scheme 2, the carbocation intermediate formed by the cleavage of the O_5-C_6 bond could be considered unstabilized carbocations, so the cleavage of the O_5-C_6 bond may be a photo-heterolysis control process rather than a thermal heterolysis process.[50] Therefore, the protonation of excited state β-LA may directly help induce the cleavage of the O_5-C_6 bond and is hence proposed as being the predominant pathway (as shown in Scheme 2).

It is worth noting that the conversion from β-LA into α-LA only takes place in aqueous solutions. Previous studies of the photophysics and photochemistry of β-LA were conducted in organic solvents by nanosecond laser flash photolysis[19−22] and found that β-^{3}LA will be quenched by hydrogen donors and L-tryptophan, L-tryptophan, methyl ester, L-tyrosine, L-tyrosine methyl ester, and L-cysteine to form the corresponding radical pair resulting from an initial electron transfer from the amino acids or their esters to the excited quinone that was followed by a fast proton transfer. However, in aqueous solutions, a different reaction occurs to convert β-LA into α-LA. It has been noted that β-LA can act as an anticancer drug that can inhibit the growth of sarcoma tumors in mice[3] and exhibits cytotoxicity to leukemia cells[4] and to human cancers such as breast, colon, prostate, and lung.[5−14] All of these studies were performed in physiological and biological conditions, and the previous studies on β-LA in the organic solvents do not appear to explain the phototoxiciy mechanism of β-LA to the cancer cells because of the different microenvironments. In fact, the

DOI: 10.1021/acs.joc.5b00086
J. Org. Chem. 2015, 80, 7340−7350

aqueous solutions are more like biological conditions. Some previous studies proposed that the mechanism of cytotoxicity in cancer cells is due to NAD(P)H quinine oxidoreductase-1 performing a two-electron reduction of β-LA to generate its hydroquinone.[12,15−17] However, we found that the protonation of O_9 will drive β-LA to convert into α-LA after photoexcitation in aqueous solution. Hooker[43] pointed out that β-LA will transform into α-LA in the presence of hydrogen chloride acidic solution in the ground electronic state, and our similar experiments with ground state β-LA also demonstrated that adding acid can convert it into α-LA, with about 90% conversion efficiency in acidic solution. Measurement by microelectrodes found that the microenvironment is often more acidic in tumors than in normal tissues.[51] This indicates that it is probable that β-LA tends to convert into α-LA in the cancer cells' microenvironment. Therefore, the cytotoxicity in cancer cells for β-LA is probably caused, at least in part, by some of its conversion into α-LA. α-LA has been demonstrated to be a strong candidate for the development of drugs to treat resistant cell lines with hyperactivity against multi-drug-resistant tumors with lower expression of topoisomerase II.[52,53] It can induce DNA cleavage mediated by topoisomerase II, which is an essential enzyme that interconverts different topological forms of DNA and is the target for some anticancer drugs.[54,55] In brief, our time-resolved spectroscopic investigation of the excited state reaction in aqueous solutions and examination of the ground state reaction in acidic aqueous solution of β-LA indicate that under these two conditions a noticeable amount of β-LA can be converted to α-LA. The cytotoxicity and phototoxicity of β-LA in biological systems will likely depend on the pH of the microenvironment and the presence or absence of photoexcitation of β-LA.

CONCLUSION

The present work reported a fs-TA, ns-TA, and ns-TR^3 spectroscopic investigation of the photophysical and photochemical reactions of β-LA in MeCN and aqueous solutions. For comparison, the photoreactions of the parent compound NQ were also studied by fs-TA in MeCN and aqueous solutions in order to help better understand the role of water and the pyran ring in the photochemistry of β-LA in aqueous solutions. ISC processes were observed for NQ in both MeCN and 1:1 MeCN/H_2O mixed solutions with time constants of about 7 ps. The ISC process of β-LA takes place in MeCN to produce the β-^{3}LA species within 29 ps. In contrast, a photoinduced protonation of the carbonyl group at the β position takes place for the singlet excited state of β-LA with the assistance of water in aqueous solutions. The protonation is the initial step to lead to the conversion of some β-LA to α-LA in water-rich solutions. After protonation of the carbonyl group at the β position, the photochemical heterolysis control cleavage of the oxygen−carbon bond (O_5−C_6) on the pyran ring appears to allow the formation of an unstabilized carbocation intermediate, which can then attack the oxygen of the alcohol group (O_9) and lead to a cyclization reaction to form the singlet excited state of α-LA that then undergoes ISC to generate the triplet state of α-LA that was observed in the ns-TA and ns-TR^3 experiments. The details of the ultrafast events and possible role of a nearby conical intersection that lead to the formation of the triplet state of α-LA observed in the ns-TA and ns-TR^3 experiments remain somewhat ambiguous, and further work is planned to address this in the future. The photochemically produced triplet state of α-LA then formed the ground singlet state of the α-lapachone final product. We also observed that some β-lapachone can be converted to α-lapachone on the ground electronic state when a strong acid is added to an aqueous solution of β-lapachone. Our present study indicates that some β-lapachone can be converted to α-lapachone by photoconversion in aqueous solutions by a water-assisted excited state reaction or by an acid-assisted ground electronic state reaction. We briefly discussed the implications of these new results in aqueous solutions for the phototoxicity and cyctotoxicity of β-lapachone in biological systems.

EXPERIMENTAL AND SECTION

The sample of β-LA was synthesized following a literature procedure, and its spectroscopic and spectrometric properties are in full accord with the structure proposed; the characterization spectra and data are provided in the Supporting Information. NQ and spectroscopic grade MeCN were purchased and used to prepare the sample solutions. Unless specified, all of the mixed solvent ratios are of volume ratio. Perchloric acid ($HClO_4$) was used to adjust the pH value of the aqueous solutions.

Femtosecond Transient Absorption Experiment. The fs-TA experiments were done by employing an experimental setup and methods detailed previously,[56] and only a brief description is provided here. Fs-TA measurements were done using a femtosecond regenerative amplified Ti:sapphire laser system, in which the amplifier was seeded with the 120 fs laser pulses from an oscillator laser system. The laser probe pulse was produced by utilizing ∼5% of the amplified 800 nm laser pulses to generate a white-light continuum (350−800 nm) in a CaF_2 crystal, and then this probe beam was split into two parts before traversing the sample. One probe laser beam goes through the sample, while the other probe laser beam goes to the reference spectrometer in order to monitor the fluctuations in the probe beam intensity. For the present experiments, the sample solution was excited by a 267 nm pump beam (the third harmonic of the fundamental 800 nm from the regenerative amplifier). The 40 mL solutions were studied in a flowing 2 mm path-length cuvette with an absorbance of 1 at 267 nm throughout the data acquisition.

Nanosecond Transient Absorption Experiment. The ns-TA measurements were carried out with a LP920 laser flash spectrometer provided by Edinburgh Instruments Ltd. The probe light source is a 450 W ozone-free Xe arc lamp with 10 Hz to a single shot operation versatile sample chamber with an integral controller, high-speed pump and probe port shutters, sample holder, and filter holders, which produces a continuous spectrum between 280 and 800 nm. Measurements of the ns-TA spectra were performed according to the following procedure. The fresh sample solutions were excited by a Q-switched Nd:YAG laser (fourth harmonic line at λ = 266 nm). The probe light from a pulsed xenon arc lamp was passed through various optical elements, samples, and a monochromator before being detected by a fast photomultiplier tube and recorded with a TDS 3012C digital signal analyzer. In the kinetics mode, a photomultiplier detector or InGaAs PIN detector is used and the transient signal acquired using a fast, high-resolution oscilloscope. In the spectral mode, an array detector is fitted to the spectrograph exit port to measure a full range of wavelengths simultaneously. Unless specified otherwise, the ns-TA experiments were performed in air-saturated solutions and the sample solutions were made up to have an absorbance of 1 at 266 nm.

Nanosecond Time-Resolved Resonance Raman Experiments. The ns-TR^3 experiments were done using an experimental apparatus and methods discussed in detail previously,[57,58] and only a short description will be given here. The pump laser pulse with a wavelength of 266 nm generated from the fourth harmonic of a Nd:YAG nanosecond pulsed laser, a 309.1 nm probe laser pulse produced from the first anti-Stokes hydrogen Raman-shifted laser line from the third (355 nm) harmonic, and a 368.9 nm probe laser pulse produced from the second anti-Stokes hydrogen Raman-shifted laser line from the second (532 nm) harmonic were employed in the TR^3

DOI: 10.1021/acs.joc.5b00086
J. Org. Chem. 2015, 80, 7340−7350

experiments. The two Nd:YAG lasers were synchronized electronically by a pulse delay generator to control the time delay of pump and probe lasers, and the time delay between the laser pulses was monitored by a fast photodiode and a 500 MHz oscilloscope. The time resolution for the TR^3 experiments was approximately 10 ns. The pump and probe laser beams were lightly focused onto the sampling system, and the Raman light was collected using reflective optics into a spectrometer, whose grating dispersed the light onto a liquid-nitrogen-cooled CCD detector. The Raman signal was acquired for 10−30 s by the CCD before reading out in the interfaced PC computer, and 10−30 scans of the signal were accumulated to produce a resonance Raman spectrum. The TR^3 spectra presented here were obtained by the subtraction of a resonance Raman spectrum with negative time delay of −100 ns (probe-before-pump spectrum) from the resonance Raman spectrum with a positive time delay (pump−probe spectrum). The TR^3 spectra in this work were calibrated by the known MeCN solvent's Raman bands with an estimated accuracy of (5 cm^{-1}). Samples of the β-LA solutions were prepared to have a UV absorption of ∼1 at 266 nm in a 1 mm path-length cuvette and then were used in the TR^3 experiments.

Density Functional Theory Calculations. DFT calculations were performed employing the (U)B3LYP method with a 6-311G** basis set. The Raman spectra were found by computing the Raman intensities from transition polarizabilities computed by numerical differentiation, with an assumed zero excitation frequency. A Lorentzian function with a 15 cm^{-1} bandwidth for the vibrational frequencies and a frequency scaling factor of 0.974 was used in the comparison of the calculated results with the experimental spectra. TD-DFT was used to calculate the excitation energies and oscillator strengths, and the simulation of UV−vis spectra of selected intermediates and excited state was obtained from (U)B3LYP DFT calculations employing a 6-311G** basis set in PCM solvent mode. No imaginary frequency modes were observed at the stationary states of the optimized structures. All of the reactions have been explored by optimizing the structures of the reactant (RC), transition states (TS), and product complexes (PC). Transition states were located using the Berny algorithm. Frequency calculations at the same level of theory have also been performed to identify all of the stationary points as minima for transition states (one imaginary frequency). Intrinsic reaction coordinates were calculated for the transition states to confirm that the relevant structures connect the two relevant minima. All of the calculations were done using the Gaussian 03 program suite[59] operated on the high-performance computing cluster (HPCPOWER2) at the University of Hong Kong.

■ ASSOCIATED CONTENT

Supporting Information

Additional fs-TA and ns-TA spectra and data obtained after photoexcitation of NQ and β-LA in MeCN and aqueous solutions of varying water concentration and pH values. Optimized geometries, Cartesian coordinates, total energies, and vibrational zero-point energies for the optimized geometry from the (U)B3LYP/6-311G** calculations for the compounds and intermediates considered in this paper. The Supporting Information is available free of charge on the ACS Publications website at DOI: 10.1021/acs.joc.5b00086.

■ AUTHOR INFORMATION

Corresponding Author

*E-mail: phillips@hku.hk.

Author Contributions

§L.D. and M.-D.L. contributed equally to this work.

Notes

The authors declare no competing financial interest.

■ ACKNOWLEDGMENTS

This work was supported by grants from the Research Grants Council of Hong Kong (HKU 7035/13P) to D.L.P. Partial support from the Grants Committee Areas of Excellence Scheme (AoE/P-03/08) and the Special Equipment Grant (SEG HKU/07) are also gratefully acknowledged.

■ REFERENCES

(1) Docampo, R.; Lopes, J. N.; Cruz, F. S.; de Souza, W. *Exp. Parasitol.* **1977**, *42*, 142−149.

(2) Docampo, R.; Cruz, F. S.; Boveris, A.; Muniz, R. P. A.; Esquivel, D. M. S. *Arch. Biochem. Biophys.* **1978**, *186*, 292−297.

(3) Docampo, R.; Cruz, F. S.; Boveris, A.; Muniz, R. P. A.; Esquivel, D. M. S. *Biochem. Pharmacol.* **1979**, *28*, 723−728.

(4) Schaffnersabba, K.; Schmidtruppin, K. H.; Wehrli, W.; Schuerch, A. R.; Wasley, J. W. F. *J. Med. Chem.* **1984**, *27*, 990−994.

(5) Luo, X. Q.; Patel, M.; Li, L. S.; Deberardinis, R.; Boothman, D. A. *Cancer Res.* **2013**, *73*, 4614.

(6) Luo, X. Q.; Li, L. S.; Huang, X. M.; Cao, L. F.; Moore, Z.; Deberardinis, R.; Brekken, R.; Gerson, S.; Lu, L. L.; Boothman, D. A. *Cancer Res.* **2013**, *73*, 3344.

(7) Park, M. T.; Song, M. J.; Lee, H.; Oh, E. T.; Choi, B. H.; Jeong, S. Y.; Choi, E. K.; Park, H. J. *PLoS. One* **2011**, *6*, e25976.

(8) Li, L. S.; Bey, E. A.; Dong, Y.; Meng, J. R.; Patra, B.; Yan, J. S.; Xie, X. J.; Brekken, R. A.; Barnett, C. C.; Bornmann, W. G.; Gao, J. M.; Boothman, D. A. *Clin. Cancer Res.* **2011**, *17*, 275−285.

(9) Imanishi, M.; Yoshida, S.; Mizuno, K. *J. Pharmacol. Sci.* **2011**, *115*, 234p−234p.

(10) Hori, T.; Kondo, T.; Lee, H.; Song, C. W.; Park, H. J. *Int. J. Hyperthermia* **2011**, *27*, 53−62.

(11) Planchon, S. M.; Pink, J. J.; Tagliarino, C.; Bornmann, W. G.; Varnes, M. E.; Boothman, D. A. *Exp. Cell Res.* **2001**, *267*, 95−106.

(12) Pink, J. J.; Planchon, S. M.; Tagliarino, C.; Varnes, M. E.; Siegel, D.; Boothman, D. A. *J. Biol. Chem.* **2000**, *275*, 5416−5424.

(13) Wuerzberger, S. M.; Pink, J. J.; Planchon, S. M.; Byers, K. L.; Bornmann, W. G.; Boothman, D. A. *Cancer Res.* **1998**, *58*, 1876−1885.

(14) Planchon, S. M.; Wuerzberger, S.; Frydman, B.; Witiak, D. T.; Hutson, P.; Church, D. R.; Wilding, G.; Boothman, D. A. *Cancer Res.* **1995**, *55*, 3706−3711.

(15) Lamberti, M. J.; Rumie Vittar, N. B.; de Carvalho da Silva, F.; Ferreira, V. F.; Rivarola, V. A. *Phytomedicine* **2013**, *20*, 1007−1012.

(16) Byun, S. J.; Son, Y.; Cho, B. H.; Chung, H. T.; Pae, H. O. *J. Clin. Biochem. Nutr.* **2013**, *52*, 106−111.

(17) Park, E. J.; Choi, K. S.; Kwon, T. K. *Chem.-Biol. Interact.* **2011**, *189*, 37−44.

(18) Bentle, M. S.; Bey, E. A.; Dong, Y.; Reinicke, K. E.; Boothman, D. A. *J. Mol. Histol.* **2006**, *37*, 203−218.

(19) Netto-Ferreira, J. C.; Lhiaubet-Vallet, V.; de Oliveira Bernardes, B.; Ferreira, A. B. B.; Miranda, M. A. *Photochem. Photobiol.* **2009**, *85*, 153−159.

(20) Netto-Ferreira, J. C.; Bernardes, B.; Ferreira, A. B. B.; Miranda, M. A. *Photoch. Photobio. Sci.* **2008**, *7*, 467−473.

(21) Ci, X. H.; Silveira da Silva, R.; Nicodem, D.; Whitten, D. G. *J. Am. Chem. Soc.* **1989**, *111*, 1337−1343.

(22) Ci, X. H.; Dasilva, R. S.; Goodman, J. L.; Nicodem, D. E.; Whitten, D. G. *J. Am. Chem. Soc.* **1988**, *110*, 8548−8550.

(23) Netto-Ferreira, J. C.; Lhiaubet-Vallet, V.; da Silva, A. R.; da Silva, A. M.; Ferreira, A. B. B.; Miranda, M. A. *J. Braz. Chem. Soc.* **2010**, *21*, 966−972.

(24) Netto-Ferreira, J. C.; Lhiaubet-Vallet, V.; Bernardes, B.; Buarque, A. B.; Ferreiraa, A. B. B.; Miranda, M. A. *Photoch. Photobio. Sci.* **2014**, *13*, 1655−1660.

(25) Armendáriz-Vidales, G.; Hernández-Muñoz, L. S.; González, F. J.; de Souza, A. A.; de Abreu, F. C.; Jardim, G. A. M.; da Silva, E. N., Jr.; Goulart, M. O. F.; Frontana, C. *J. Org. Chem.* **2014**, *79*, 5201−5208.

(26) Bell, R. P. *The Proton in Chemistry*; Chapman and Hall: London, 1973.

DOI: 10.1021/acs.joc.5b00086
J. Org. Chem. 2015, 80, 7340−7350

(27) Klán, P.; Wirz, J. *Photochemistry of Organic Compounds*; John Wiley & Sons, Ltd.: New York, 2009; pp 183−226.
(28) Li, M. D.; Huang, J.; Liu, M.; Li, S.; Ma, J.; Phillips, D. L. *J. Phys. Chem. B* **2015**, *119*, 2241−2252.
(29) Li, M. D.; Yeung, C. S.; Guan, X. G.; Ma, J.; Li, W.; Ma, C.; Phillips, D. L. *Chem. - Eur. J.* **2011**, *17*, 10935−10950.
(30) Hubig, S. M.; Bockman, T. M.; Kochi, J. K. *J. Am. Chem. Soc.* **1997**, *119*, 2926−2935.
(31) Becker, R. S.; Natarajan, L. V. *J. Phys. Chem.* **1993**, *97*, 344−349.
(32) Li, M. D.; Li, W.; Ma, J.; Su, T.; Liu, M.; Du, Y.; Phillips, D. L. *J. Phys. Chem. A* **2011**, *115*, 14168−14174.
(33) Aloise, S.; Ruckebusch, C.; Blanchet, L.; Rehault, J.; Buntinx, G.; Huvenne, J. P. *J. Phys. Chem. A* **2008**, *112*, 224−231.
(34) Wagner, P. J.; Truman, R. J.; Puchalski, A. E.; Wake, R. *J. Am. Chem. Soc.* **1986**, *108*, 7727−7738.
(35) Wagner, P. J.; Siebert, E. J. *J. Am. Chem. Soc.* **1981**, *103*, 7329−7335.
(36) Wagner, P. J.; Puchalski, A. E. *J. Am. Chem. Soc.* **1980**, *102*, 6177−6178.
(37) Toscano, J. P., Ed. *Structure and Reactivity of Organic Intermediates as Revealed by Time-Resolved Infrared Spectroscopy*; Wiley: New York, 2001; Vol. *26*.
(38) Schwartz, B. J.; Peteanu, L. A.; Harris, C. B. *J. Phys. Chem.* **1992**, *96*, 3591−3598.
(39) Webb, S. P.; Philips, L. A.; Yeh, S. W.; Tolbert, L. M.; Clark, J. H. *J. Phys. Chem.* **1986**, *90*, 5154−5164.
(40) Webb, S. P.; Yeh, S. W.; Philips, L. A.; Tolbert, M. A.; Clark, J. H. *J. Am. Chem. Soc.* **1984**, *106*, 7286−7288.
(41) de Lucas, N. C.; Correa, R. J.; Albuquerque, A. C. C.; Firme, C. L.; Garden, S. J.; Bertoti, A. R.; Netto-Ferreira, J. C. *J. Phys. Chem. A* **2007**, *111*, 1117−1122.
(42) Marx, D.; Tuckerman, M. E.; Hutter, J.; Parrinello, M. *Nature* **1999**, *397*, 601−604.
(43) Hooker, S. C. *J. Chem. Soc., Trans.* **1892**, *61*, 611−650.
(44) Ramseier, M.; Senn, P.; Wirz, J. *J. Phys. Chem. A* **2003**, *107*, 3305−3315.
(45) Netto-Ferreira, J. C.; Lhiaubet-Vallet, V.; Bernardes, B. O.; Ferreira, A. B. B.; Miranda, M. A. *Phys. Chem. Chem. Phys.* **2008**, *10*, 6645−6652.
(46) Ettlinger, M. G. *J. Am. Chem. Soc.* **1950**, *72*, 3090−3095.
(47) Ribeiro, F. W.; Pinto, M. C. F. R.; Pinto, A. V. *J. Braz. Chem. Soc.* **1990**, *1*, 55−57.
(48) Li, M. D.; Du, Y.; Chuang, Y. P.; Xue, J.; Phillips, D. L. *Phys. Chem. Chem. Phys.* **2010**, *12*, 4800−4808.
(49) Li, M. D.; Su, T.; Ma, J.; Liu, M.; Liu, H.; Li, X.; Phillips, D. L. *Chem. - Eur. J.* **2013**, *19*, 11241−11250.
(50) Buck, A. T.; Beck, C. L.; Winter, A. H. *J. Am. Chem. Soc.* **2014**, *136*, 8933−8940.
(51) Griffiths, J. R. *Br. J. Cancer* **1991**, *64*, 425−427.
(52) Krishnan, P.; Bastow, K. F. *Biochem. Pharmacol.* **2000**, *60*, 1367−1379.
(53) Krishnan, P.; Bastow, K. F. *Cancer Chemother. Pharmacol.* **2001**, *47*, 187−198.
(54) Frydman, B.; Marton, L. J.; Sun, J. S.; Neder, K.; Witiak, D. T.; Liu, A. A.; Wang, H. M.; Mao, Y.; Wu, H. Y.; Sanders, M. M.; Liu, L. F. *Cancer Res.* **1997**, *57*, 620−627.
(55) Fortune, J. M.; Velea, L.; Graves, D. E.; Utsugi, T.; Yamada, Y.; Osheroff, N. *Biochemistry* **1999**, *38*, 15580−15586.
(56) Li, M. D.; Ma, J.; Su, T.; Liu, M.; Yu, L.; Phillips, D. L. *J. Phys. Chem. B* **2012**, *116*, 5882−5887.
(57) Du, L.; Zhu, R.; Xue, J.; Du, Y.; Phillips, D. L. *J. Raman Spectrosc.* **2015**, *46*, 117−125.
(58) Xue, J.; Du, L.; Zhu, R.; Huang, J.; Phillips, D. L. *J. Org. Chem.* **2014**, *79*, 3610−3614.
(59) Frisch, M. J.; Trucks, G. W.; Schlegel, H. B.; Scuseria, G. E.; Robb, M. A.; Cheeseman, J. R.; Montgomery, J. A., Jr.; Vreven, T.; Kudin, K. N.; Burant, J. C.; Millam, J. M.; Iyengar, S. S.; Tomasi, J.; Barone, V.; Mennucci, B.; Cossi, M.; Scalmani, G.; Rega, N.; Petersson, G. A.; Nakatsuji, H.; Hada, M.; Ehara, M.; Toyota, K.; Fukuda, R.; Hasegawa, J.; Ishida, M.; Nakajima, T.; Honda, Y.; Kitao, O.; Nakai, H.; Klene, M.; Li, X.; Knox, J. E.; Hratchian, H. P.; Cross, J. B.; Bakken, V.; Adamo, C.; Jaramillo, J.; Gomperts, R.; Stratmann, R. E.; Yazyev, O.; Austin, A. J.; Cammi, R.; Pomelli, C.; Ochterski, J. W.; Ayala, P. Y.; Morokuma, K.; Voth, G. A.; Salvador, P.; Dannenberg, J. J.; Zakrzewski, V. G.; Dapprich, S.; Daniels, A. D.; Strain, M. C.; Farkas, O.; Malick, D. K.; Rabuck, A. D.; Raghavachari, K.; Foresman, J. B.; Ortiz, J. V.; Cui, Q.; Baboul, A. G.; Clifford, S.; Cioslowski, J.; Stefanov, B. B.; Liu, G.; Liashenko, A.; Piskorz, P.; Komaromi, I.; Martin, R. L.; Fox, D. L.; Keith, T.; Al-Laham, M. A.; Peng, C. Y.; Nanayakkara, A.; Challacombe, M.; Gill, P. M. W.; Johnson, B.; Chen, W.; Wong, M. W.; Gonzalez, C.; Pople, J. A. *Gaussian 03*, revision C.02; Gaussian, Inc.: Pittsburgh, PA, 2004.

DOI: 10.1021/acs.joc.5b00086
J. Org. Chem. 2015, 80, 7340−7350